Supporting Information

Manipulation of Ionic Liquid Anion–Solute–Antisolvent Interactions for the Purification of Acetaminophen

Cameron C. Weber, Andreas J. Kunov-Kruse, Robin D. Rogers and Allan S. Myerson

Experimental Section

Materials. 1-Ethyl-3-methylimidazolium acetate ([EMIM][OAc]), 1-ethyl-3-methylimidazolium bis(trifluoromethanesulfonyl)imide ([EMIM][NTf$_2$]), 1-butyl-3-methylimidazolium tetrafluoroborate ([BMIM][BF$_4$]), 1-(2-hydroxyethyl)-3-methylimidazolium tetrafluoroborate ([EtOHMIM][BF$_4$]) and 1-butylpyridinium tetrafluoroborate ([BPy][BF$_4$]) were all purchased from Iolitec and stored in a drybox under a nitrogen atmosphere. Acetaminophen (AAP), toluene, 4-aminophenol (4-AP), 4-nitrophenol (4-NP), 4'-chloroacetanilide (4'-CA), 1,1,1,3,3,3-hexafluoroisopropanol (HFIPA) and acetic acid (AcOH) were purchased from Sigma Aldrich and used as received. Ethanol (EtOH), acetone and dimethylsulfoxide (DMSO) were purchased from VWR.

IL mixtures were prepared by directly weighing the appropriate mass of each IL into a vial and mixing using a Vortex mixer.

Solubility Experiments. In a typical solubility experiment, 1 g solvent was added to excess solid and the resultant suspension stirred for 24 h using a rare earth magnetic stirrer. The temperature was maintained at 25 ± 0.1 °C by means of a Peltier heating system in an Avantium Crystal16 instrument. The suspension was passed through a 0.20 μm syringe filter and the filtrate diluted in deuterated acetone. The mole fraction solubility was determined by NMR.

NMR Analysis of Solute Interactions. IL samples for neat analysis were prepared by weighing the appropriate amount of solute into the IL. The solution was then stirred using a rare earth magnetic stirrer for at least 1 h then transferred to an NMR tube and analyzed neat using a sealed, co-axially inserted capillary containing acetone-d_6 as a lock and chemical shift reference. NMR

experiments were conducted on a Bruker AVANCE III 400 MHz spectrometer fitted with an automatically tunable broadband BBO probe.

Infrared Spectroscopy. Solutions of AAP, EtOH, AcOH and HFIPA in [EMIM][OAc]$_{0.25}$[NTf$_2$]$_{0.75}$ were prepared by directly weighing both components into a vial and stirring until a homogeneous solution results. Spectra were obtained using a Smiths IdentifyIR spectrometer over the range 650–4000 cm^{-1}.

Powder X-ray Diffraction. Powder XRD was performed using a PANalytical X'Pert Pro diffractometer over the range 5–50° 2θ using a Cu K$_\alpha$ source with a total collection time of 10 min 37 sec and sample stage rotation of 15 rpm. Solid samples were pressed flat onto a zero background sample holder without grinding to prevent polymorph transformation.

IL Crystallization Experiments. In a typical crystallization experiment, AAP (1.00 g) and impurity (0.11 g) were dissolved with stirring in a vial fitted with a septum containing [EMIM][OAc]$_{0.25}$[NTf$_2$]$_{0.75}$ (5.00 g). The temperature was maintained at 25 °C by means of a recirculating water bath and the appropriate volume of antisolvent (AcOH (0.43, 0.86 or 1.7 mL) or HFIPA (0.90, 1.8 or 3.6 mL)) rapidly injected. The solution was allowed to stir for 1 h before being filtered and the solid washed with dichloromethane (2 × 5 mL) and dried at the pump. A similar procedure was used for [EMIM][OAc]$_{0.50}$[NTf$_2$]$_{0.50}$ except 2.33 g AAP and 0.26 g impurity were used and the antisolvent volumes adjusted according to the appropriate molar ratio. To examine the effect of antisolvent addition rate, a modification was used where AcOH was added to solutions of AAP and 4-AP, 4-NP or 4'-CA in [EMIM][OAc]$_{0.50}$[NTf$_2$]$_{0.50}$ over 1 h using a syringe pump with 0.41 mL dispensed over the first 20 min, 0.61 mL in the following 20 min and the remaining 1.02 mL in the final 20 min, the resultant suspension was then allowed to stir for an additional 30 min followed by the same filtration procedure as for the rapid addition.

Crystallization from DMSO and water. AAP (4.60 g) and impurity (0.51 g) were dissolved in DMSO (5.00 g) in a recirculated water bath maintained at 25 °C. Water (5.0 mL) was rapidly added to the stirred solution, the resultant suspension allowed to stir for 1 h before being filtered,

washed with dichloromethane (2 × 5 mL) and dried at the pump. Literature solubility data were used to determine saturation concentrations.[1]

Crystallization from toluene and acetone. AAP (0.294 g) and impurity (0.033 g) were dissolved with stirring in an acetone (6.0 mL) / toluene (2.8 mL) mixture in a recirculated water bath maintained at 25 °C. Toluene (10.0 mL) was rapidly added to the stirred solution, the resultant suspension allowed to stir for 1 h before being filtered, washed with dichloromethane (2 × 5 mL) and dried at the pump. Literature solubility data were used to determine saturation concentrations.[2]

HPLC Analysis. The HPLC instrument (Agilent 1100) was equipped with a UV diode array detector. The column used was a YMC-Pack ODS-A 150 × 4.6 mm i.d. column packed with 3 μm particles with 12 nm pore size (YMC America Inc.). The detection wavelength was set at 275 nm for AAP and 4-AP, 254 nm for 4'-CA and 230 nm for 4-NP. Samples were analyzed using an isocratic method with a 30:70 methanol:water mobile phase containing 0.3% trifluoroacetic acid with a 10 μL injection and 1 mL min^{-1} flow rate. Analysis run times were 5 min for 4-AP, 20 min for 4-NP and 35 min for 4'-CA.

LC-MS Analysis. LC-MS analysis of residual IL was conducted on an Agilent 6460 Triple Quadrupole LC-MS coupled to an Agilent 1290 Infinity HPLC. [EMIM] cation analysis was conducted by a multiple reaction monitoring (MRM) approach monitoring the formation of the methylimidazolium fragment from the EMIM cation. The HPLC method used a 2 μL injection onto a 2 × 20 mm i.d. Gemini C18 column with 3 μm particles at 0.3 mL min^{-1} flow rate with a gradient method progressing linearly from 95:5 20 mM ammonium acetate in water (pH 9.4): acetonitrile to 47.5:52.5 buffer:acetonitrile after 0.5 min followed by a linear gradient back to the original mobile phase between 1.1 and 2.5 min. [NTf$_2$] anion analysis was conducted by monitoring the fragmentation of [NTf$_2$] into the trifluoromethanesulfonylimide anion. The anion analysis used a 2 μL injection onto a 2 × 50 mm Luna NH$_2$ column with 3 μm particles at a 0.3 mL min^{-1} flow rate with an isocratic 3 min 95:5 20 mM ammonium acetate in water (pH 9.4): acetonitrile method. Samples were prepared by dissolution and dilution in 30:70 methanol:water with 0.1% formic acid.

Solubility of AAP and 4-AP in Different ILs

Table S1. Solubility data for the dissolution of AAP and 4-AP at 25 °C.

IL	AAP (mol%)	4-AP (mol%)
[EMIM][NTf$_2$]	1.3	1.0
[BMIM][BF$_4$]	9.7	6.6
[EMIM][OAc]	_[a]	_[a]
[BPy][BF$_4$]	10.0	7.1
[EtOHMIM][BF$_4$]	4.0	5.1

[a] Solubility > 40 wt%. Solution too viscous to stir before solubility limit was reached.

Solubility of AAP and 4-AP with different concentrations of [EMIM][OAc] in [EMIM][NTf$_2$]
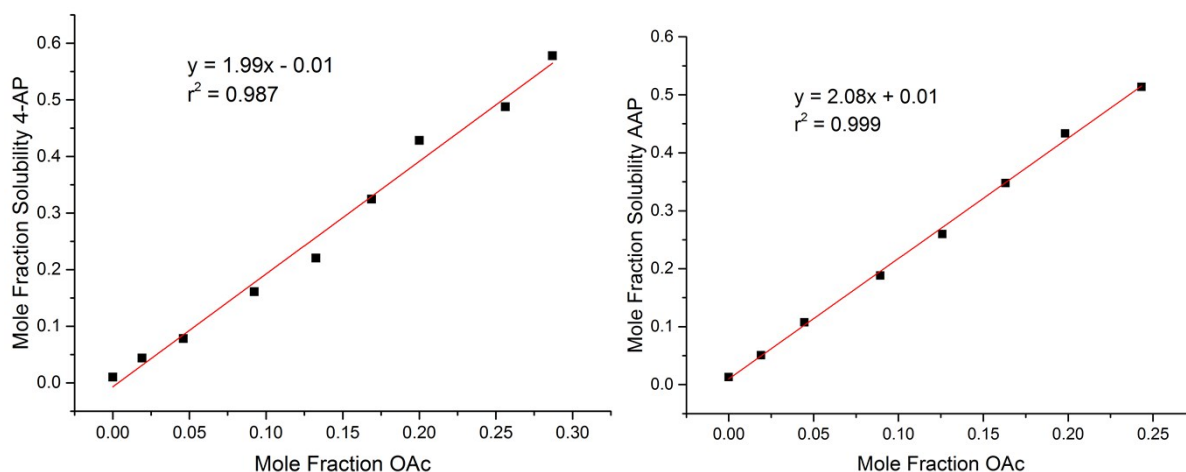
Figure S1. Correlation between the [OAc]$^-$ concentration of the solution and Left: 4-AP solubility, Right: AAP solubility.
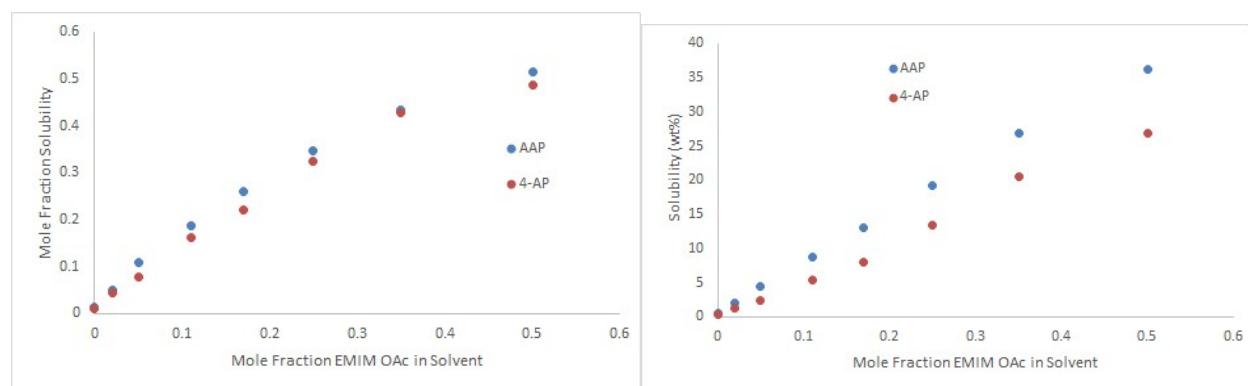
Figure S2. Left: Mole fraction solubility of AAP and 4-AP versus composition of [EMIM][OAc]$_x$[NTf$_2$]$_{1-x}$ solvent. Right: Wt% solubility of AAP and 4-AP versus composition of [EMIM][OAc]$_x$[NTf$_2$]$_{1-x}$ solvent.

NMR Analysis of Neat AAP, EtOH, AcOH and HFIPA in [EMIM][OAc]$_{0.25}$[NTf$_2$]$_{0.75}$
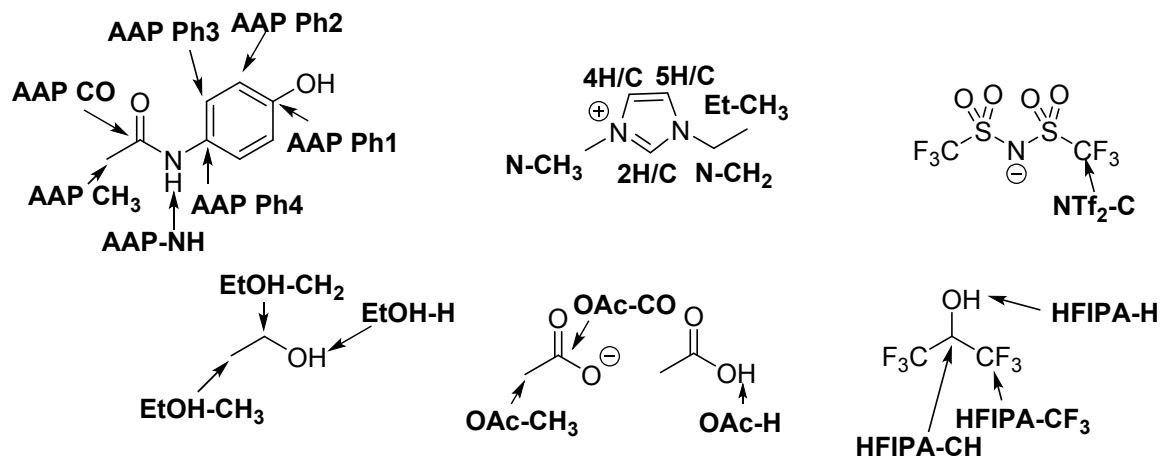
Figure S3. H and C nuclei labelled as they will be referred to in the below NMR tables.

Table S2. ^{1}H chemical shifts of [EMIM][OAc]$_{0.25}$[NTf$_2$]$_{0.75}$ and AAP in ppm with the pure IL, [EMIM][NTf$_2$] and [EMIM][OAc] as references. Ratios are AAP:[OAc] anion molar ratios. See Figure S3 for signal labelling.

Sample	2H	4H	5H	N-CH$_3$	N-CH$_2$	Et-CH$_3$	OAc-CH$_3$	AAP-Ph2	AAP-Ph3	AAP-CH$_3$	AAP-NH
[EMIM][NTf$_2$]	7.47	6.33	6.41	2.83	3.16	0.43	-	-	-	-	-
[EMIM][OAc]	9.75	7.47	7.65	3.15	3.43	0.41	0.64	-	-	-	-
[EMIM][OAc]$_{0.25}$[NTf$_2$]$_{0.75}$	8.45	6.56	6.66	2.89	3.21	0.43	0.82	-	-	-	-
0.5:1 AAP	8.06	6.45	6.53	2.84	3.16	0.40	0.87	5.71	6.29	1.03	9.74
1:1 AAP	7.80	6.29	6.44	2.79	3.11	0.37	0.91	5.72	6.28	1.02	9.24
2:1 AAP	7.49	6.22	6.29	2.69	3.00	0.30	0.95	5.69	6.22	0.99	8.55

Table S3. ^{13}C chemical shifts of [EMIM][OAc]$_{0.25}$[NTf$_2$]$_{0.75}$ and AAP in ppm with the pure IL, [EMIM][NTf$_2$] and [EMIM][OAc] as references. Ratios are AAP:[OAc] anion molar ratios. See Figure S3 for signal labelling.

Sample	2C	4C	5C	N-CH$_3$	N-CH$_2$	Et-CH$_3$	OAc-CH$_3$	OAc-CO	NTf$_2$-C	AAP-Ph1	AAP-Ph2	AAP-Ph3	AAP-Ph4	AAP-CH$_3$	AAP-CO
[EMIM][NTf$_2$]	135.65	121.69	123.40	35.41	44.69	14.05	-	-	119.75	-	-	-	-	-	-
[EMIM][OAc]	138.67	122.89	124.31	35.44	44.21	15.45	25.66	174.82	-	-	-	-	-	-	-
[EMIM][OAc]$_{0.25}$[NTf$_2$]$_{0.75}$	137.02	121.84	123.48	35.31	44.52	14.35	25.05	176.18	119.76	-	-	-	-	-	-
0.5:1 AAP	136.49	121.78	123.45	35.36	44.57	14.30	24.68	176.68	119.76	155.32	115.36	122.21	130.51	22.84	169.08
1:1 AAP	136.11	121.71	123.41	35.37	44.58	14.24	24.42	177.15	119.76	155.11	115.36	122.22	130.42	22.91	169.11
2:1 AAP	135.69	121.63	123.36	35.36	44.59	14.18	24.15	177.94	119.76	154.74	115.35	122.45	130.29	22.96	169.36

Table S4. ^{1}H chemical shifts of [EMIM][OAc]$_{0.25}$[NTf$_2$]$_{0.75}$ and EtOH in ppm. Ratios are EtOH:[OAc] anion molar ratios. See Figure S3 for signal labelling.

Sample	2H	4H	5H	N-CH$_3$	N-CH$_2$	Et-CH$_3$	OAc-CH$_3$	EtOH-CH$_2$	EtOH-CH$_3$	EtOH-H
1:1 EtOH	8.31	6.57	6.66	2.93	3.25	0.47	0.86	2.53	0.05	5.57
2:1 EtOH	8.18	6.56	6.65	2.94	3.27	0.49	0.88	2.55	0.08	5.17
4:1 EtOH	8.09	6.60	6.68	2.99	3.32	0.55	0.93	2.62	0.15	4.72
8:1 EtOH	8.09	6.67	6.74	3.07	3.40	0.64	1.02	2.71	0.25	4.42

Table S5. ^{13}C chemical shifts of [EMIM][OAc]$_{0.25}$[NTf$_2$]$_{0.75}$ and EtOH in ppm. Ratios are EtOH:[OAc] anion molar ratios. See Figure S3 for signal labelling.

Sample	2C	4C	5C	N-CH$_3$	N-CH$_2$	Et-CH$_3$	OAc-CH$_3$	OAc-CO	NTf$_2$-C	EtOH-CH$_2$	EtOH-CH$_3$
1:1 EtOH	136.78	121.84	123.49	35.35	44.55	14.39	24.79	176.52	119.76	56.19	17.88
2:1 EtOH	136.61	121.87	123.54	35.41	44.62	14.43	24.59	176.84	119.80	56.35	17.86
4:1 EtOH	136.44	121.92	123.60	35.48	44.69	14.48	24.35	177.28	119.85	56.56	17.82
8:1 EtOH	136.36	122.02	123.70	35.58	44.78	14.57	24.17	177.73	119.92	56.82	17.80

Table S6. ^{1}H chemical shifts of [EMIM][OAc]$_{0.25}$[NTf$_2$]$_{0.75}$ and AcOH in ppm. Ratios are AcOH:[OAc] anion molar ratios. See Figure S3 for signal labelling.

Sample	2H	4H	5H	N-CH$_3$	N-CH$_2$	Et-CH$_3$	OAc-CH$_3$	OAc-H
1:1 AcOH	7.99	6.51	6.59	2.91	3.24	0.47	0.86	13.91
2:1 AcOH	7.82	6.50	6.57	2.93	3.26	0.50	0.93	12.70
4:1 AcOH	7.78	6.53	6.60	2.98	3.31	0.56	1.03	11.57
8:1 AcOH	7.80	6.58	6.64	3.04	3.37	0.62	1.12	10.98

Table S7. ^{13}C chemical shifts of [EMIM][OAc]$_{0.25}$[NTf$_2$]$_{0.75}$ and AcOH in ppm. Ratios are AcOH:[OAc] anion molar ratios. See Figure S3 for signal labelling.

Sample	2C	4C	5C	N-CH$_3$	N-CH$_2$	Et-CH$_3$	OAc-CH$_3$	OAc-CO	NTf$_2$-C
1:1 AcOH	136.43	121.83	123.52	35.44	44.64	14.35	22.45	175.68	119.79
2:1 AcOH	136.17	121.85	123.57	35.53	44.72	14.35	21.53	175.38	119.83
4:1 AcOH	136.01	121.91	123.64	35.60	44.80	14.38	20.86	175.32	119.87
8:1 AcOH	135.97	122.01	123.75	35.68	44.89	14.45	20.52	175.79	119.94

Table S8. ^{1}H chemical shifts of [EMIM][OAc]$_{0.25}$[NTf$_2$]$_{0.75}$ and HFIPA in ppm. Ratios are HFIPA:[OAc] anion molar ratios. See Figure S3 for signal labelling.

Sample	2H	4H	5H	N-CH$_3$	N-CH$_2$	Et-CH$_3$	OAc-CH$_3$	HFIPA- CH	HFIPA-H
1:1 HFIPA	7.94	6.46	6.54	2.88	3.21	0.45	0.84	3.87	10.50
2:1 HFIPA	7.67	6.38	6.45	2.86	3.16	0.45	0.86	3.67	9.16
4:1 HFIPA	7.56	6.33	6.40	2.87	3.20	0.48	0.92	3.61	7.34
8:1 HFIPA	7.47	6.28	6.34	2.88	3.20	0.52	0.98	3.58	5.86

Table S9. ^{13}C chemical shifts of $[EMIM][OAc]_{0.25}[NTf_2]_{0.75}$ and HFIPA in ppm. Ratios are HFIPA:[OAc] anion molar ratios. See Figure S3 for signal labelling.

Sample	2C	4C	5C	N-CH$_3$	N-CH$_2$	Et-CH$_3$	OAc-CH$_3$	OAc-CO	NTf$_2$-C	HFIPA-CH	HFIPA-CF$_3$
1:1 HFIPA	136.24	121.73	123.41	35.27	44.57	14.16	23.58	176.98	119.73	122.95	68.14
2:1 HFIPA	135.80	121.70	123.40	35.26	44.64	14.02	22.68	178.27	119.74	122.61	68.23
4:1 HFIPA	135.47	121.66	123.37	35.17	44.68	13.84	22.16	179.70	119.70	122.21	68.32
8:1 HFIPA	135.04	121.67	123.38	35.04	44.77	13.59	21.82	180.84	119.59	121.91	68.48

Comparison of the NMR data for pure $[EMIM][NTf_2]$, $[EMIM][OAc]$ and $[EMIM][OAc]_{0.25}[NTf_2]_{0.75}$ with data obtained in the presence of AAP, EtOH, AcOH and HFIPA demonstrates a number of informative trends. Firstly, the upfield shift of the 2H and 2C resonances in the $[EMIM]^+$ cation are indicative of weaker interactions between the IL cation and anion. This is observed for all hydrogen bond donating species added although notably the maximum change in chemical shift increases in the order EtOH < AcOH < HFIPA for the antisolvents, i.e. the order of hydrogen bond strength. This suggests that the stronger the hydrogen bonding interactions between the added compound and the $[OAc]^-$, the greater the disruption of $[EMIM]^+$ cation - $[OAc]^-$ anion interactions, as would be expected. The extent of the upfield shift of 4H/C and 5H/C resonances also follows this antisolvent trend, although interestingly there is only a very small shift for AcOH and in EtOH there is actually a slight downfield shift. Given the weaker hydrogen bonding interactions and reduced probability of the $[OAc]^-$ ion occupying the 4H/C and 5H/C positions in the absence of additives,[3] this variation in chemical shift may be due to a superposition of other factors such as ring stacking and other subtle effects.[4]

Other notable variations in chemical shift include the O–H ^1H resonance in EtOH, AcOH and HFIPA which all shift upfield with increasing antisolvent concentration. The observed resonance is the weighted average of the underlying hydrogen bonding modes and hence the apparent upfield shift is caused by the saturation of the strongest hydrogen bonding modes as the antisolvent concentration is increased. The magnitude of the upfield shift gives insight into the strength of the interaction with the IL as this represents the difference between self-association of the antisolvent and its association with the IL. Notably this difference is largest for HFIPA and smallest for EtOH, which accords with their relative hydrogen bond donating capacity. Such an analysis is more

difficult to conduct for AAP as the saturation of the strong hydrogen bonding modes would occur at the limit of solubility. In addition, the O–H resonance of AAP could not be detected as the signal was too broad. Nonetheless, the N-H group of AAP depicts a similar upfield shift indicating that it is involved in hydrogen bonding interactions with the IL, in accordance with the observations in the IR spectra.

The effect of hydrogen bonding interactions on the IL anions could be followed by examining the ^{13}C chemical shift of OAc-CO and NTf_2-C. As anticipated from the solubility data, evidence of a strong hydrogen bonding interaction between AAP and the $[OAc]^-$ can be observed as a significant downfield shift of the OAc-CO resonance. No change in the NTf_2-C signal is observed, consistent with hydrogen bonding interactions being negligible between AAP and the $[NTf_2]^-$ anion. For the antisolvents, a pronounced downfield shift of the OAc-CO resonance was observed for both EtOH and HFIPA, with the shift for HFIPA being 3.1 ppm greater reiterating the enhanced strength of hydrogen bonds between HFIPA and the $[OAc]^-$ anion. No significant effect on the OAc-CO resonance could be detected for AcOH as the signal is an average of both AcOH and the $[OAc]^-$ anion. Both EtOH and AcOH lead to a small downfield shift for the NTf_2-C resonance indicating some interactions with the $[NTf_2]^-$ anion even at low antisolvent ratios. HFIPA does not lead to any pronounced NTf_2-C variation until it is present at ratios greater than 2:1 relative to the $[OAc]^-$ anion and subsequently leads to an upfield shift which may be suggestive of fluorous interactions between the $[NTf_2]^-$ anion and HFIPA dominating after $[OAc]^-$ becomes saturated.

IR Analysis of [EMIM][OAc]$_{0.25}$[NTf$_2$]$_{0.75}$ with AAP, EtOH, AcOH and HFIPA
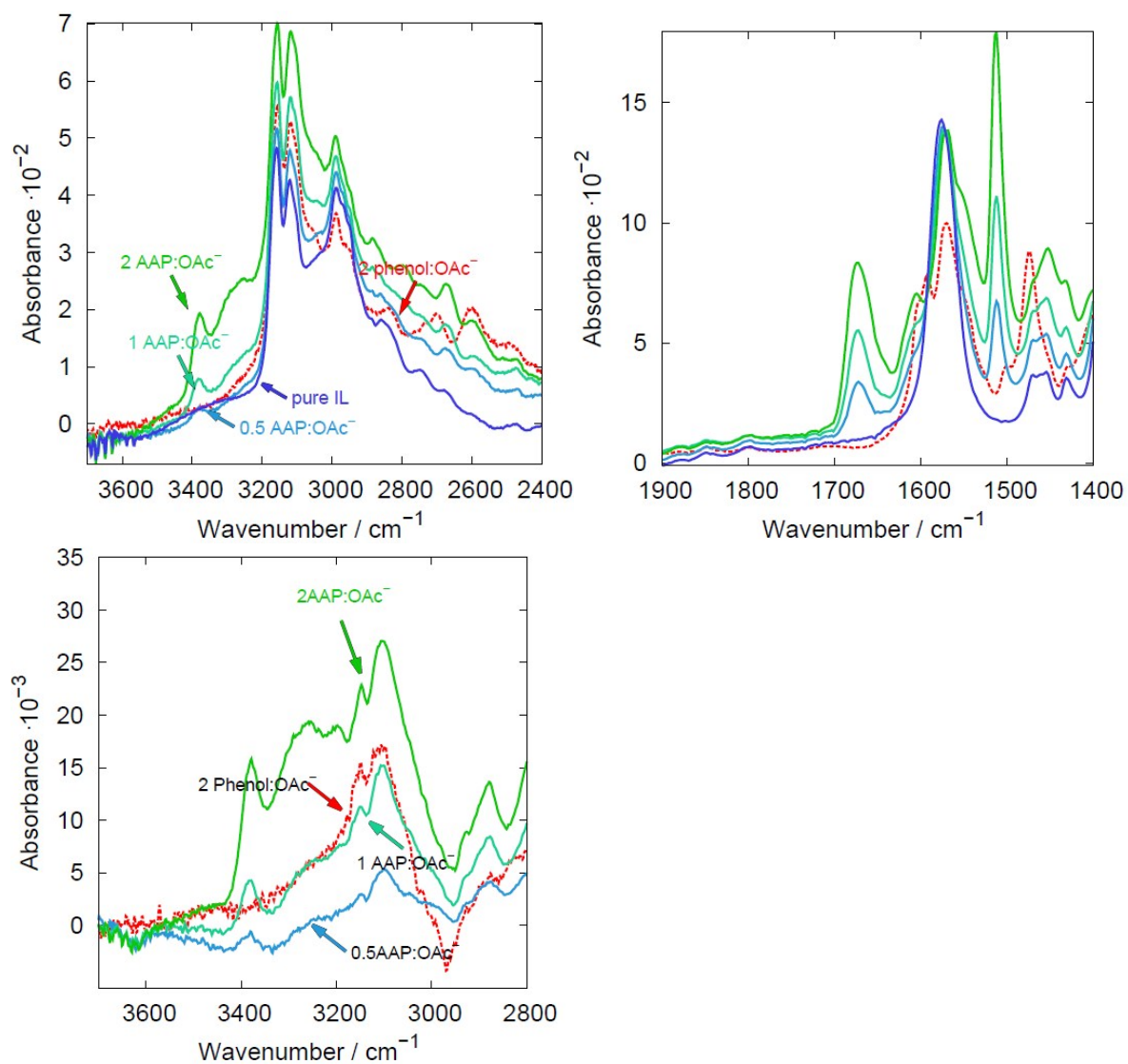
Figure S4. IR spectra of [EMIM][OAc]$_{0.25}$[NTf$_2$]$_{0.75}$ with 0.5:1, 1:1 and 2:1 mole ratios of AAP:[OAc] anion with the spectrum of the pure IL for reference and that of 2:1 phenol:[OAc]$^-$ anion for the identification of N-H modes. (Clockwise from top left): 2400–3700 cm^{-1} region; 1400–1900 cm^{-1} region and difference spectrum of 2800–3700 cm^{-1} region substracted from the pure IL spectrum.

For the subsequent discussion, $\nu_{A\text{-}B}$ refers to an A-B stretching mode and $\delta_{A\text{-}B}$ refers to an A-B bending mode. From the 2400–3700 cm^{-1} region, it is evident by comparison with phenol that the bands at ~3380 cm^{-1} correspond to the amide $\nu_{N\text{-}H}$ and the shoulders at ~3250 cm^{-1} with phenolic $\nu_{O\text{-}H}$. The rest of this region is complicated by absorptions corresponding to the IL, hence a

difference spectrum was obtained between each sample and the pure IL. These difference spectra indicate additional bands at ~3200, 3150 and 3100 cm^{-1}. The 3150 and 3100 cm^{-1} modes are also present in the phenol sample which suggests they arise from different ν_{O-H} hydrogen bonding modes. The lack of a 3200 cm^{-1} mode for phenol implies that this likely represents a ν_{N-H} mode from the amide in AAP which is shifted to lower wavenumbers due to hydrogen bonding interactions. Notably this 3200 cm^{-1} mode becomes relatively more intense at higher AAP concentrations indicating that NH hydrogen bonding may be of secondary importance to that exhibited by the phenolic group.

It is also worth considering modes arising from the IL, particularly the ν_{CH} from 2800–3200 cm^{-1}. For ILs with strong hydrogen bond accepting anions (such as [OAc]$^-$), the ν_{CH} from the 2 position on the imidazolium ring is strong and around 3000 cm^{-1} due to strong cation–anion interactions, while for weaker hydrogen bond acceptors such as [NTf$_2$]$^-$, this band is weaker and towards 3150 cm^{-1}, an effect that has been observed for other ILs.[5] In the difference spectra in Figure S4, a valley close to 3000 cm^{-1} is observed in all spectra and increases with increasing AAP loading. This indicates that the cation–anion interactions are weakened as a result of AAP addition, consistent with the NMR findings.

Finally, in the 1400–1900 cm^{-1} region the peaks 1673 cm^{-1} (strong, $\nu_{C=O}$), 1645 cm^{-1} (shoulder, δ_{N-H}) and 1604 cm^{-1} (shoulder, δ_{O-H}) are observed in the AAP spectra with no discernable changes. The major change in these spectra is the shift of the antisymmetric ν_{O-C-O} stretch of the [OAc]$^-$ anion from 1576 cm^{-1} in the pure IL to a 1549 cm^{-1} shoulder in the 2:1 AAP:[OAc]$^-$ sample. The remaining band initially at 1574–1568 cm^{-1} is likely due to δ_{C-H} modes from the aromatic hydrogens on the [EMIM]$^+$ cation. These modes are less sensitive to the hydrogen bonding interactions and the observed decrease in their intensity is due to dilution of the IL.
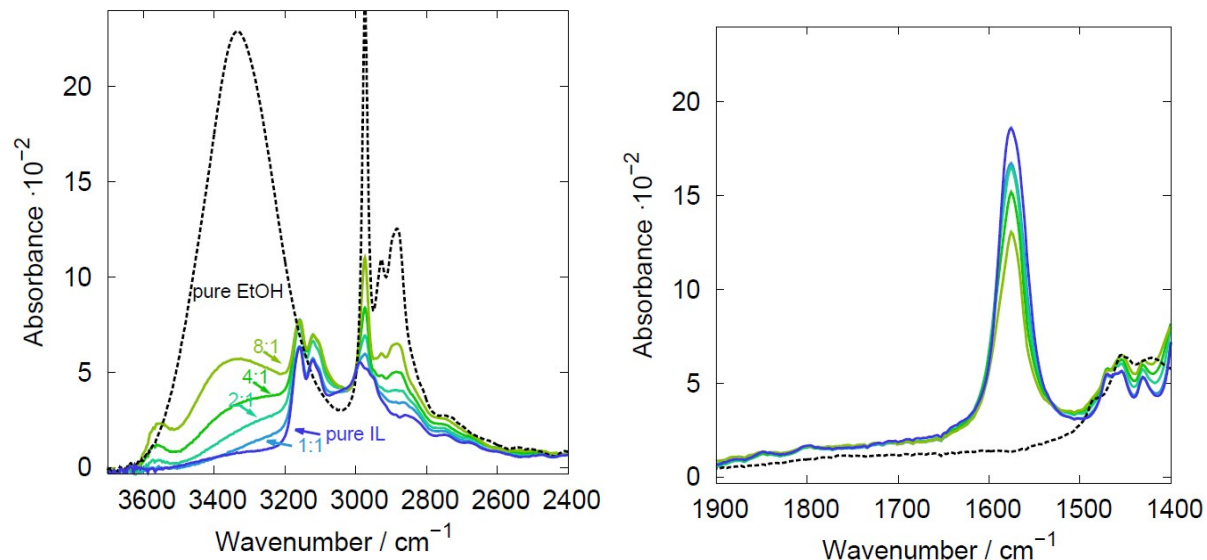
Figure S5. IR spectra of [EMIM][OAc]$_{0.25}$[NTf$_2$]$_{0.75}$ with 1:1, 2:1, 4:1 and 8:1 mole ratios of EtOH:[OAc] anion with the spectra of the pure compounds for reference. (Left): 2400–3700 cm^{-1} region; (Right) 1400–1900 cm^{-1} region.
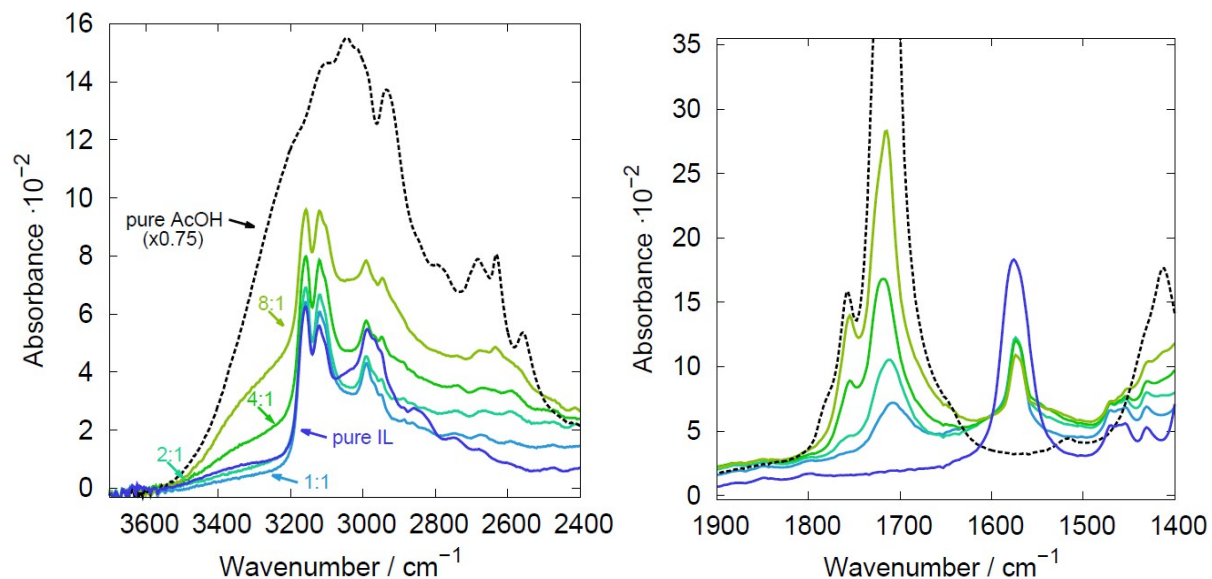
Figure S6. IR spectra of [EMIM][OAc]$_{0.25}$[NTf$_2$]$_{0.75}$ with 1:1, 2:1, 4:1 and 8:1 mole ratios of AcOH:[OAc] anion with the spectra of the pure compounds for reference. (Left): 2400–3700 cm^{-1} region; (Right) 1400–1900 cm^{-1} region.
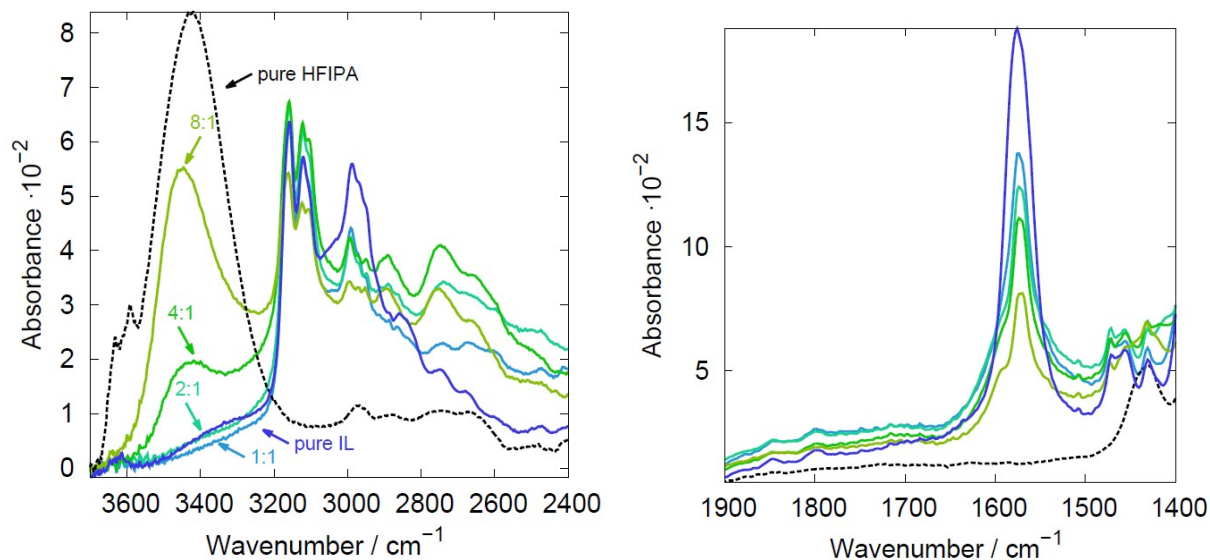
Figure S7. IR spectra of [EMIM][OAc]$_{0.25}$[NTf$_2$]$_{0.75}$ with 1:1, 2:1, 4:1 and 8:1 mole ratios of HFIPA:[OAc] anion with the spectra of the pure compounds for reference. (Left): 2400–3700 cm^{-1} region; (Right) 1400–1900 cm^{-1} region.

The 1400–1900 cm^{-1} region in Figure S5 is relatively straightforward to interpret with the major peak at 1576 cm^{-1} corresponding to overlapping ν_{O-C-O} and δ_{C-H} bands as discussed above. No significant shift of these bands is observed in the presence of EtOH, suggesting hydrogen bonding with the [OAc]$^-$ anion is substantially weaker than that observed for AAP. The 2400–3700 cm^{-1} region yields similar results with very little variation in the [EMIM]$^+$ ν_{C-H} modes. The most notable change is the formation of two EtOH ν_{O-H} modes with a broad band at ~3200 cm^{-1} for 1:1 EtOH:[OAc]$^-$ shifting to higher wavenumbers with increased EtOH loading and a narrower peak ~3550 cm^{-1}. The former mode corresponds to EtOH engaged in a hydrogen bond donating interaction, likely with the [OAc]$^-$ anion of the IL. Although, as noted above, this interaction appears to be sufficiently weak that it does not alter the electronics of the [OAc]$^-$ anion or its interaction with the [EMIM]$^+$ cation substantially. The higher wavenumber mode is more difficult to assign, although could arise from 'free' EtOH not involved in any significant hydrogen bonding interactions. As native EtOH consists of a hydrogen bonded network, the shift to higher wavenumbers probably arises from EtOH diluted in the IL but not strongly interacting with any of the IL ions or other EtOH molecules. Collectively these IR spectra indicate that while EtOH does engage in hydrogen bonding interactions, these are relatively weak compared to AAP.

Figure S6 demonstrates that AcOH engages in hydrogen bonding interactions with the IL, with the ν_{O-H} bands shifting to significantly lower wavenumbers for the 1:1 and 2:1 AcOH:[OAc]$^-$ ratios, overlapping with the ν_{C-H} from the [EMIM]$^+$ cation. At higher AcOH concentrations, these bands shift to higher wavenumbers suggesting a saturation of the stronger hydrogen bonding interactions. The intensity of the ν_{C-H} modes of the [EMIM]$^+$ cation around 3000 cm^{-1} also weakens at 1:1 and 2:1 AcOH:[OAc]$^-$ ratios, as observed for AAP, indicating weaker [EMIM]$^+$ – anion interactions. In the 1400–1900 cm^{-1} region the ν_{O-C-O} of AcOH at ~1700 cm^{-1} noticeably shifts to lower wavenumbers in the 1:1 and 2:1 AcOH:[OAc]$^-$ cases. The ν_{O-C-O} of [OAc]$^-$ also shifts to lower wavenumbers and reduces substantially in intensity with added AcOH, due to changes in symmetry and strong hydrogen bonding interactions. These results are consistent with the NMR studies that suggest AcOH forms stronger hydrogen bonding interactions with the [OAc]$^-$ anions than EtOH does.

From Figure S7 it can be seen that the main ν_{O-H} region for HFIPA lies around 3430 cm^{-1}. This mode is clearly absent in 1:1 and 2:1 HFIPA:[OAc]$^-$ samples with the appearance of a new band around 2700 cm^{-1} which is not present in either pure HFIPA or pure IL. The new band is indicative of very strong hydrogen bond donating interactions by the HFIPA and notably this new band reaches maximum intensity at 4:1 HFIPA:[OAc]$^-$, in accordance with the solubility minimum observed. The ν_{C-H} at ~3000 cm^{-1} is also substantially weakened in the presence of HFIPA, indicating weaker cation–anion interactions in the IL as discussed previously. The ν_{O-C-O} and δ_{C-H} overlapping modes behave in a similar fashion to the AAP samples with the δ_{C-H} bands being simply diluted while the ν_{O-C-O} modes shift to lower wavenumbers indicating strong hydrogen bonding interactions. Collectively these IR data are in agreement with the NMR results that strong hydrogen bonding interactions are present in solution and the order of those interactions with the antisolvents is EtOH < AcOH < HFIPA.

Wt% Solubility Curves for AAP in [EMIM][OAc]$_{0.25}$[NTf$_2$]$_{0.75}$
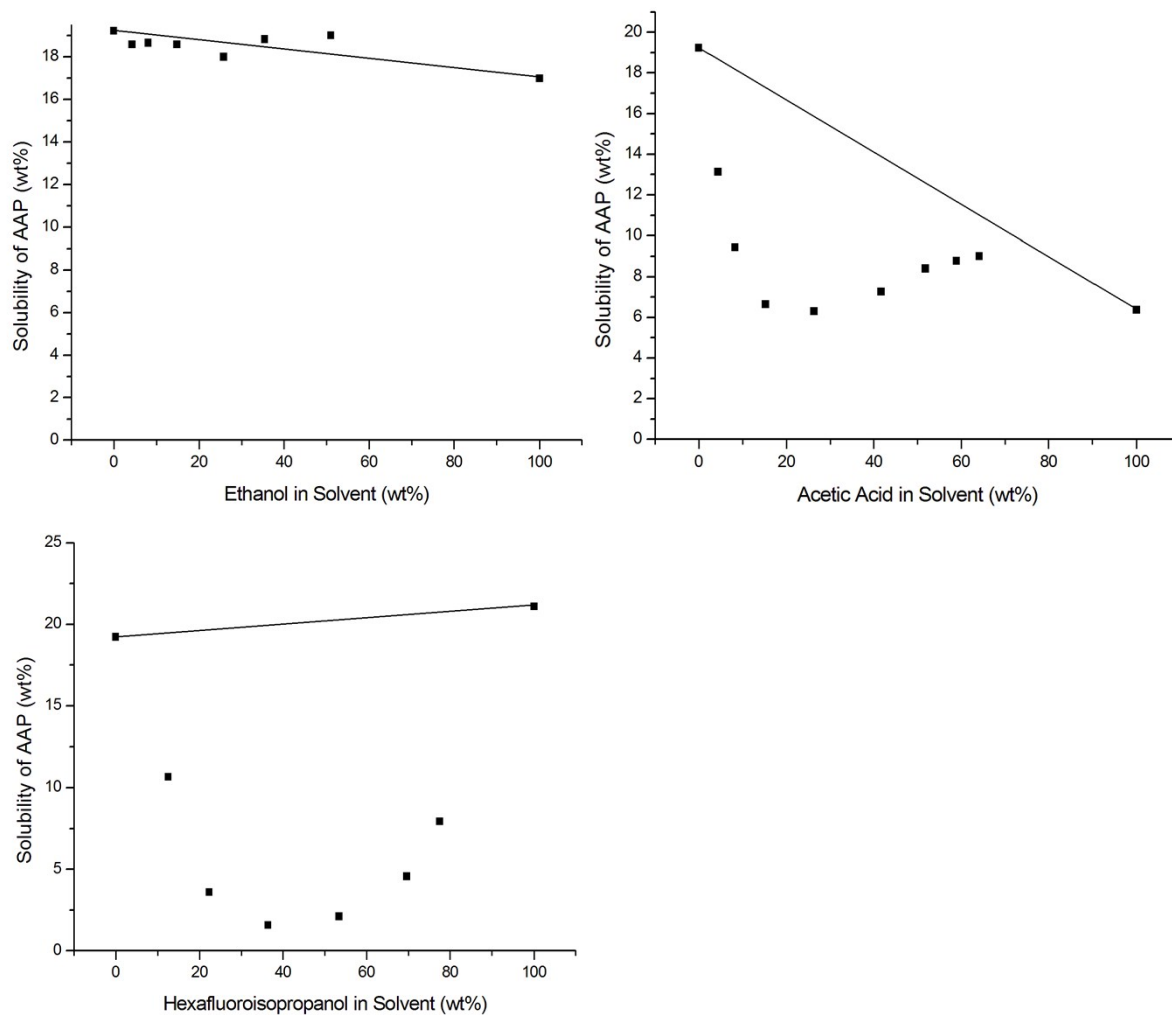
Figure S8. Solubility of AAP in mixed solvents containing [EMIM][OAc]$_{0.25}$[NTf$_2$]$_{0.75}$ and (clockwise from top left): EtOH, AcOH and HFIPA in terms of mass.

Solubility Curves for AAP in [EMIM][OAc]$_{0.50}$[NTf$_2$]$_{0.50}$
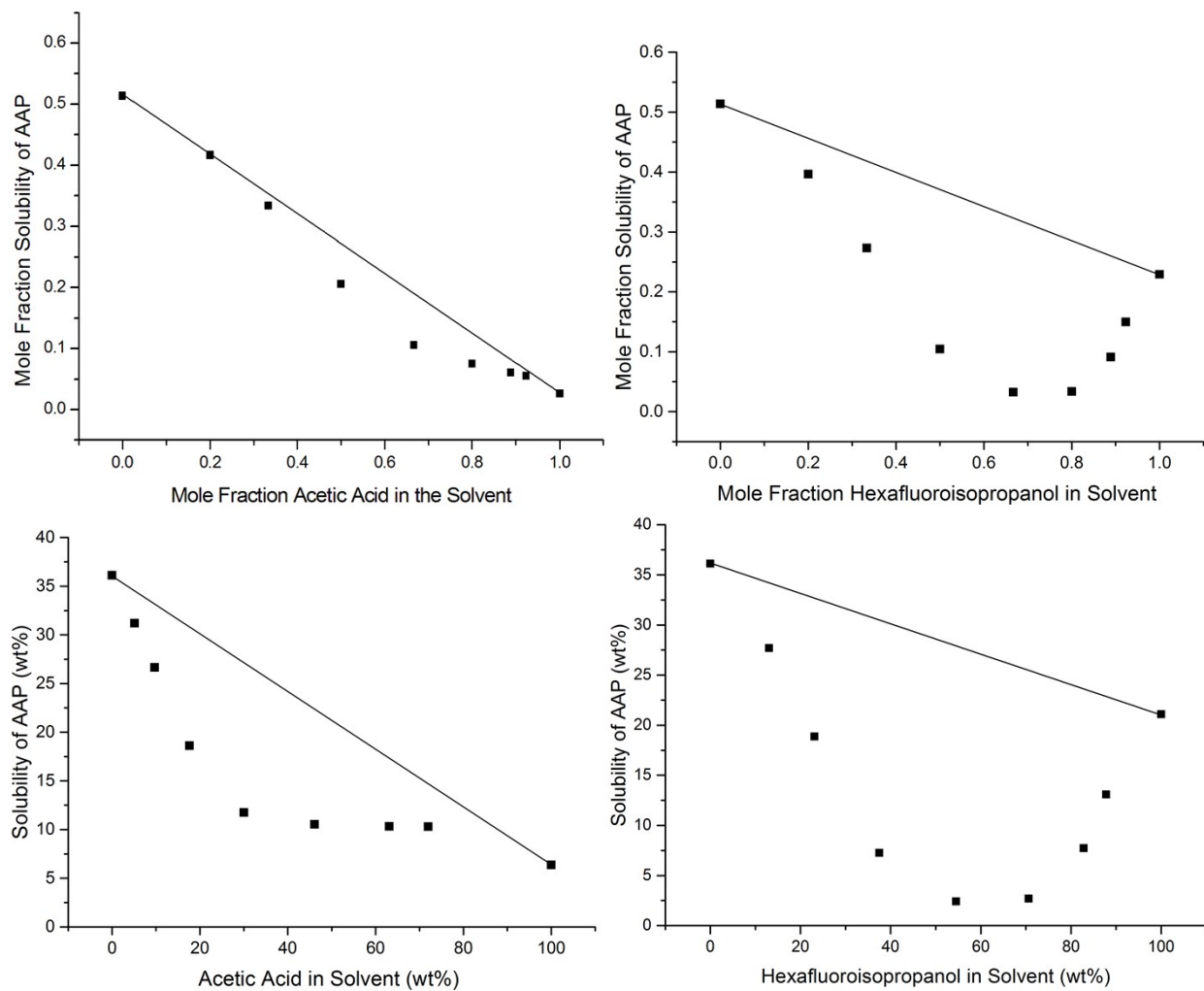
Figure S9. Solubility curves for AAP in mixed solvents containing [EMIM][OAc]$_{0.50}$[NTf$_2$]$_{0.50}$ and (clockwise from top left): AcOH (mole fraction), HFIPA (mole fraction), AcOH (mass) and HFIPA (mass).

Powder XRD of AAP Samples
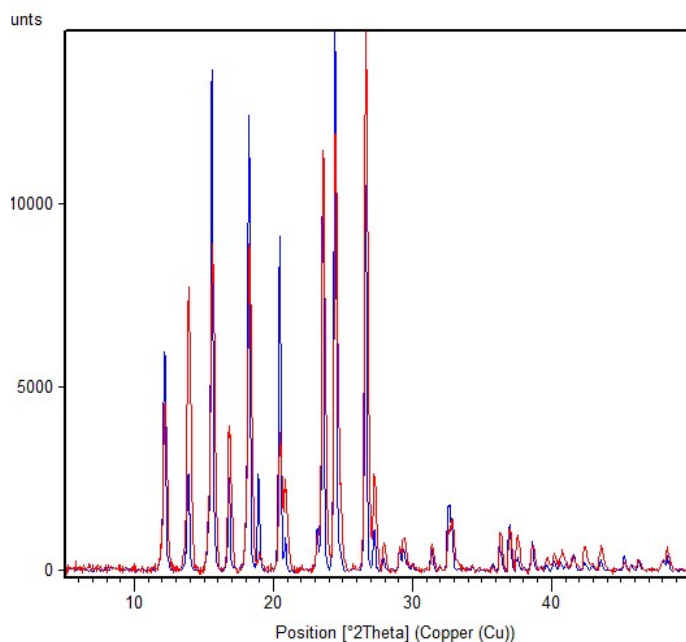
Figure S10. Overlaid powder XRD diffractograms of commercial AAP form 1 (red) and a representative sample of AAP crystallized from $[EMIM][OAc]_x[NTf_2]_{1-x}$ ILs (blue). Intensity differences are due to preferential orientation effects as samples were not ground prior to analysis to avoid the potential interconversion of polymorphs on grinding. Identical peak positions were observed for all crystallization products.

Comparison of Crystallization Outcome with Antisolvent Addition Rate

Table S10. Comparison of impurity inclusion for samples of AAP with 10 wt% impurity crystallized from $[EMIM][OAc]_{0.50}[NTf_2]_{0.50}$ by slow or rapid addition of AcOH. Reported errors are standard deviations from replicate experiments.

Addition Rate	4-AP Inclusion (wt%)	4-NP Inclusion	4'-CA Inclusion
Rapid (Instantaneous)	0.41 ± 0.02	0.13 ± 0.02	1.24 ± 0.09
Slow (1 h addition)	0.57 ± 0.05	0.14 ± 0.08	0.96 ± 0.06

While there is a slight discrepancy between the values obtained by rapid and slow addition of antisolvent, particularly for 4'-CA, the magnitude of the difference relative to experimental error is small and does not suggest a strong dependence of the impurity inclusion on the rate of antisolvent addition.

LC-MS IL Analysis for [EMIM][OAc]$_{0.25}$[NTf$_2$]$_{0.75}$

Table S11. Residual IL inclusion and composition of residual [EMIM][OAc]$_x$[NTf$_2$]$_{1-x}$ for AAP crystallized from [EMIM][OAc]$_{0.25}$[NTf$_2$]$_{0.75}$ with 4-AP impurity as determined by LC-MS. Errors are standard deviations from replicate experiments.

Antisolvent Ratio	IL inclusion (wt%)	x in [EMIM][OAc]$_x$[NTf$_2$]$_{1-x}$
2:1 AcOH	0.49 ± 0.14	0.79 ± 0.08
4:1 AcOH	0.206 ± 0.003	0.78 ± 0.07
8:1 AcOH	0.09 ± 0.02	0.68 ± 0.11
2:1 HFIPA	1.13 ± 0.01	0.78 ± 0.02
4:1 HFIPA	0.51 ± 0.11	0.62 ± 0.03
8:1 HFIPA	0.09 ± 0.01	0.62 ± 0.11

From Table S11, the IL inclusion in AAP decreases as the antisolvent ratio increases within AcOH and HFIPA. This is likely due to the reduced viscosity of the resultant solution which facilitates more efficient washing of the crystals. Interestingly, the ratio of [OAc]⁻ in the included ILs is much higher than in the initial solution as it increases in all cases from x = 0.25 to x > 0.6. This trend can be partially explained by the increased affinity of [EMIM][NTf$_2$] towards less polar solvents (such as dichloromethane)[6] relative to [EMIM][OAc] which would result in its more effective removal by washing. The strong intermolecular interactions between [EMIM][OAc] and AAP may also be partially responsible for the increased adherence of this IL to the AAP crystals.

^{1}H NMR Analysis of Residual IL in AAP

Table S12. Results of quantitative ^{1}H NMR analysis of residual IL in AAP crystallized from $[EMIM][OAc]_x[NTf_2]_{1-x}$ solvents with AcOH or HFIPA antisolvents. Ratios are molar ratios of antisolvent:$[OAc]^-$ anion in the IL.

Antisolvent Ratio $[EMIM][OAc]_{0.25}[NTf_2]_{0.75}$	Mole $[EMIM]^+$ / Mole AAP ($\times 10^3$)	Antisolvent Ratio $[EMIM][OAc]_{0.50}[NTf_2]_{0.50}$	Mole $[EMIM]^+$ / Mole AAP ($\times 10^3$)
2:1 AcOH	6.3 ± 1.9	2:1 AcOH	7.3 ± 2.4
4:1 AcOH	4.3 ± 1.5	4:1 AcOH	3.0 ± 0.9
8:1 AcOH	ND	8:1 AcOH	3.5 ± 0.7
2:1 HFIPA	8.8 ± 1.7	2:1 HFIPA	8.3 ± 1.9
4:1 HFIPA	6.1 ± 3.0	4:1 HFIPA	3.2 ± 1.2
8:1 HFIPA	ND	8:1 HFIPA	4.4 ± 1.0

As can be seen from the large error values, the very low mole fractions of IL in AAP (< 1 mol%) lead to substantial inherent measurement errors using NMR. From the LC-MS results for $[EMIM][OAc]_{0.25}[NTf_2]_{0.75}$ it is apparent that these NMR values qualitatively reflect the order of IL inclusion, although it is worth considering that the NMR ratios do not account for the anion speciation as even worse signal to noise is obtained. It appears from these results that the 2:1 and 4:1 AcOH and HFIPA antisolvent samples follow the same trend for $[EMIM][OAc]_{0.50}[NTf_2]_{0.50}$ as for $[EMIM][OAc]_{0.25}[NTf_2]_{0.75}$, with decreasing inclusion with increasing antisolvent. This trend does stop at 8:1 for both antisolvents where a very similar or even slightly higher level of IL inclusion is observed. The trend may be due to increased initial concentrations of [EMIM][OAc], which is more difficult to remove than $[EMIM][NTf_2]$ using the dichloromethane washing procedure, based on the LC-MS results in Table S11. The higher [EMIM][OAc] content may lead to a greater 'minimum' IL inclusion when the viscosity of the filtered solution is reduced sufficiently so that washing is no longer mass transfer limited.

Results of Crystallization from DMSO/Water and Acetone/Toluene

Table S13. Results of crystallization of AAP from the acetone/toluene antisolvent system with either 4-AP or 4-NP impurities. Errors are standard deviations from replicate experiments.

Impurity	Yield (%)	Impurity Inclusion (wt%)
4-AP	52.4 ± 1.3	0.30 ± 0.02
4-NP	54.1 ± 0.3	0.0071 ± 0.0002
4'-CA	54.0 ± 0.7	0.547 ± 0.008

Table S14. Results of crystallization of AAP from the DMSO/water antisolvent system with either 4-AP or 4-NP impurities. Errors are standard deviations from replicate experiments.

Impurity	Yield (%)	Impurity Inclusion (wt%)
4-AP	49.5 ± 0.6	0.372 ± 0.003
4-NP	45.4 ± 1.7	0.060 ± 0.004

Crystallizations from neutral solvents were conducted to compare with the purification outcomes of the IL. These antisolvent systems were selected such that isothermal antisolvent crystallizations could be conducted with yields close to those obtained by the IL systems.

Comparing Tables S13, S14 and the IL results in Figure 7 it is evident that the acetone/toluene antisolvent system gives the best purification results of the solvent systems examined for the given yields. However, crystallizations from acetone were conducted under significantly more dilute conditions due to the lower solubility of AAP in acetone compared to the IL systems or DMSO, which may be partially responsible for the reduced inclusion. The DMSO/water system was therefore used to enable a comparison with a neutral solvent system with similar crystallization capacity to the IL. The DMSO results lie within error of those obtained by crystallization from the IL system at comparable yields, suggesting that the IL approach does no worse than neutral solvents at comparable crystallization capacities. Notably, much higher yields are able to be obtained using an isothermal antisolvent crystallization from the IL than from DMSO/water. Furthermore the effect on 4'-CA inclusion was not able to be measured in DMSO due to the poor solubility of 4'-CA upon the addition of water, indicating that the IL approach has greater flexibility towards different impurity systems. It is worth considering that DMSO is a strong

hydrogen bond acceptor for a neutral solvent system and water is a strong hydrogen bond donor, which implies that the crystallization conducted is a neutral solvent equivalent to the hydrogen bond manipulation approach demonstrated for the IL. The similar mechanism may also be partially responsible for the comparable purification results obtained for 4-NP and 4-AP impurities.

References

(1)   Granberg, R. A.; Rasmuson, A. C. *J. Chem. Eng. Data* **1999**, *44*, 1391.

(2)   Granberg, R. A.; Rasmuson, A. C. *J. Chem. Eng. Data* **2000**, *45*, 478.

(3)   Bowron, D. T.; D'Agostino, C.; Gladden, L. F.; Hardacre, C.; Holbrey, J. D.; Lagunas, M. C.; McGregor, J.; Mantle, M. D.; Mullan, C. L.; Youngs, T. G. A. *J. Phys. Chem. B* **2010**, *114*, 7760.

(4)   Avent, A. G.; Chaloner, P. A.; Day, M. P.; Seddon, K. R.; Welton, T. *J. Chem. Soc. Dalton Trans.* **1994**, 3405.

(5)   Jeon, Y.; Sung, J.; Seo, C.; Lim, H.; Cheong, H.; Kang, M.; Moon, B.; Ouchi, Y.; Kim, D. *J. Phys. Chem. B* **2008**, *112*, 4735.

(6)   Wang, H.; Gurau, G.; Kelley, S. P.; Myerson, A. S.; Rogers, R. D. *RSC Adv.* **2013**, *3*, 10019.